Available online at www.sciencedirect.com
SCIENCE DIRECT®
Journal of Molecular Catalysis A: Chemical 219 (2004) 175–181
JOURNAL OF MOLECULAR CATALYSIS A: CHEMICAL
www.elsevier.com/locate/molcata

Immobilization of rhodium complexes ligated with triphenyphosphine analogs on amino-functionalized MCM-41 and MCM-48 for 1-hexene hydroformylation

Qingrong Peng, Yong Yang, Youzhu Yuan*

State Key Laboratory for Physical Chemistry of Solid Surfaces, Department of Chemistry, Xiamen University, Xiamen 361005, China

Received 6 January 2004; received in revised form 23 April 2004; accepted 6 May 2004

Available online 15 June 2004

Abstract

Two triphenylphosphine analogs, (4-*tert*-butylphenyl)diphenylphosphine (**1**) and bis-(4-*tert*-butylphenyl)phenylphosphine (**2**), have been synthesized for the preparation of Rh–P complexes with a formula of $Rh(CO)Cl(L)_2$ (*L* stands for the ligands **1** and **2**, respectively). Such Rh–P complexes were then attached to amino-group functionalized MCM-41 and MCM-48 for the hydroformylation of 1-hexene in the liquid phase. The supports and the heterogeneous catalysts were characterized by means of XRD, nitrogen adsorption–desorption, FT-IR, HRTEM and AAS. The heterogenized catalysts showed catalytic activity and normal heptanal selectivity comparable to the corresponding homogeneous ones; the advantage in the product selectivity towards the normal heptanal due to the larger cone angle of the ligands over $Rh–PPh_3$ in the homogeneous systems was also observed in the heterogeneous ones. Considerable interactions occurred between the surface amino-groups and the active rhodium species during the immobilization, resulting in highly dispersed active Rh-moieties and a significant modification in the catalytic stability.

Keywords: MCM-41; MCM-48; Immobilization; Rhodium–phosphine complexes; Cone angle; Amino-functionalization; 1-Hexene; Hydroformylation

1. Introduction

Great research interest has been shown in the immobilization of transition metal complexes on the inorganic and/or organic supports in the last several decades [1,2], although there still exist severe obstacles to overcome, especially the lower catalytic activity and selectivity and the leaching of the active metal in the course of reaction. Efforts to investigate new methods are of particular importance. An example of the progresses in this field may be ascribed to a type of catalyst consisting of a tethered complex on a supported metal. The applications of such catalysts have been successfully tested, resulting in excellent catalytic performance in the hydrogenation [3–5] and olefin hydroformylation [6]. On the other hand, due to their huge surface areas, well ordered periodic structures, and controllable pore size by varying the template molecule and/or using additives such as trimethylbenzene [7], the mesoporous molecular sieves are attractive in seeking the novel catalysts for chemical reactions. Representatively, the modification of mesoporous materials by grafting metal complexes is an important area of research in heterogeneous catalysis [8]. One of the best pathways has already been achieved by anchoring neutral ligand onto silica through covalent Si–O–Si bonds. The neutral ligands were mainly amine or phosphine functions directly grafted to the silica surface by a silylation procedure. These types of ligands permit immobilization of metal complexes through a coordination bond with metal centers. A number of studies have shown that the high concentrations of surface silanol groups (Si-OH) enable the various successes in modification of MCM-41 or MCM-48 by a host–guest interaction for catalysis purposes to achieve improved catalytic performance in terms of selectivity and even enantioselectivity due to the nano-sized pore structure with spatial confinement [9–16].

We previously used MCM-41 directly to immobilize the Wilkinson's type $Rh–PPh_3$ (PPh_3: triphenylphosphine) complex for gas-phase hydroformylation of propene and

* Corresponding author. Tel.: +86 59 2218 4565; fax: +86 59 2218 3047.
E-mail address: yzyuan@xmu.edu.cn (Y. Yuan).

1381-1169/$ – see front matter © 2004 Elsevier B.V. All rights reserved.
doi:10.1016/j.molcata.2004.05.003

the catalysts showed a higher aldehyde production [17]. In recent years, the immobilization of Rh–PPh_3 complexes onto amino-functionalized MCM-41 and MCM-48 as efficient heterogeneous catalysts for higher olefin hydroformylation has been reported by several groups [18–20]. It was found that the immobilization of such complexes could improve the catalytic selectivity and stability. Quite recently, the triphenylphosphine analogs, (4-*tert*-butylphenyl)diphenylphosphine (**1**) and bis-(4-*tert*-butylphenyl)phenylphosphine (**2**) have been synthesized for the purpose of preparing the amphiphilic phosphines for the biphasic palladium-catalyzed cleavage of undecyl allyl carbonate by Caron et al. [21] and rhodium-catalyzed hydroformylation of higher olefins by us [22]. We have found that such phosphines **1** and **2** possess larger cone angles and that the corresponding Rh-complexes are able to afford higher selectivity to normal aldehyde in olefin hydroformylation [22]. Herein, we report the immobilization of rhodium complexes ligated with **1** and **2** onto amino-functionalized MCM-41 and MCM-48 for 1-hexene hydroformylation in the liquid phase. The aim of this work is to explore the interaction of the Rh–P complexes with the amino-MCM-41/amino-MCM-48 and also to clarify the relationship between structural property of the heterogenized Rh–P complexes and the catalytic performance in hydroformylation of liquid olefins.

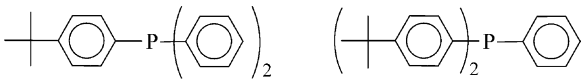

1 **2**

2. Experimental

2.1. General comments

All experiments were performed under an atmosphere of dry argon using standard Schlenk techniques. Commercially available reagents, bromo-4-*tert*-butylbenzene (Aldrich), phosphorus(III) chlorides Ph_2PCl and $PhPCl_2$ (Acros) were used without further purification. THF was distilled from sodium/benzophenone under argon before use. Solvents were purchased from Aldrich and used without further purification, unless stated. The phosphines, (4-*tert*-butylphenyl)diphenylphosphine (**1**) and bis-(4-*tert*-butylphenyl)phenylphosphine (**2**), and the rhodium complexes based on the *tert*-butyl-substituted phosphines with the general formula $Rh(CO)Cl(L)_2$ (*L* stands for the ligands of **1** or **2**) were obtained as described elsewhere [22], The rhodium complexes were designed as Rh–P**1** and Rh–P**2**, respectively.

2.2. Catalyst preparation

The mesoporous silicas MCM-41 and MCM-48 were synthesized by referring to the procedures described in literature [23]. Aminoalkylsilane-modifications of periodic mesoporous silicas were performed according to methods in literature [24,25]. In a typical synthesis, 1.5 g of MCM-41 or MCM-48 was dehydrated under vacuum at 473 K for 2 h in a Schlenk tube and then was added 50 ml of anhydrous toluene containing 2 ml of aminoalkylsilanes such as 3-aminopropytrimethoxysilane (1N-functional reagent), [3-(2-aminoethyl)-aminopropyl]-trimethoxysilane (2N-functional reagent). The mixture was filtered after being stirred for 24 h at 383 K under Ar. The solid was washed repeatedly with dry toluene and dried at 323 K under vacuum for 12 h. The functionalized silicas were designed as 1N- and 2N-support, respectively.

Immobilization of Rh–P complexes was performed by adding 1.0 g functionalized support to a solution containing the Rh–P**1** or Rh–P**2** (0.107 mol) in 50 ml of anhydrous ethanol and stirred for 16 h at room temperature under Ar. The solid powder was then washed with refluxing ethanol for 12 h, followed by filtration and drying and then stored under vacuum. The samples were designed as Rh–P**1**/1N-MCM-41, Rh–P**1**/2N-MCM-41, Rh–P**2**/1N-MCM-41, Rh–P**2**/2N-MCM-41, etc., respectively.

2.3. Characterization

The structures of phosphines and corresponding rhodium complexes were studied by infrared (FT-IR), ^{1}H- and ^{31}P-NMR spectroscopies. FT-IR spectra were measured on a Nicolet 740 spectrometer in KBr pellets with a resolution of 4 cm^{-1}. NMR spectroscopy was measured on a Varian FT Unity$^+$ 500 spectrometer at room temperature. The sample was dissolved in $CDCl_3$ before measurements. ^{31}P-NMR spectra were recorded at 202 MHz. The chemical shift was referenced to 85% H_3PO_4. ^{1}H-NMR spectra were referenced to $SiMe_4$. Powder XRD patterns were obtained at room temperature on a Rigaku Rotaflex D/Max-c diffractometer using Cu K_α radiation in 40 kV and 20 mA. Nitrogen adsorption–desorption isotherms were obtained on a Micromeritics TriStar 3000 instrument at liquid nitrogen temperature. Before measurement, about 0.4 g of sample was degassed at 393 K for 3 h. The specific surface area of the samples were calculated by using the multiple-point Brunauer–Emmett–Teller (BET) method. The pore size distribution curves were computed by using the Barret–Joyner–Halenda (BJH) method, and pore sizes were obtained from the peak positions of the distribution curves. CHN elemental analyses were performed on a Perkin-Elmer series II CHNS/O analyzer 2400. Combustion temperature was set at 1248 K. The rhodium contents of encapsulated catalysts were determined by atomic absorption spectroscopy (AAS) on a WFX-1E2 instrument. The sample was first treated with 5 ml of aqua regia at 363 K for 5–10 min, and then 5 ml of aqueous HF (5%) was added to the mixture, followed by heating at 363 K for 5–10 min. The resulting solution was diluted with water to 25 ml. High-resolution TEM images were obtained on a

Table 1
Structure property and elemental analysis data for MCM-41 and MCM-48 before and after amino-functionalization

Sample	S_{BET} ($m^2\,g^{-1}$)	Pore size (nm)	Pore volume ($ml\,g^{-1}$)	Elemental content (wt.%)	
				C	N
MCM-41	1272	2.8	0.88	–	–
1N-MCM-41	755	2.4	0.53	9.27	3.17
2N-MCM-41	702	2.3	0.48	10.42	5.15
MCM-48	1373	2.4	0.96	–	–
1N-MCM-48	858	2.3	0.30	7.18	2.27
2N-MCM-48	755	2.4	0.23	10.71	5.16

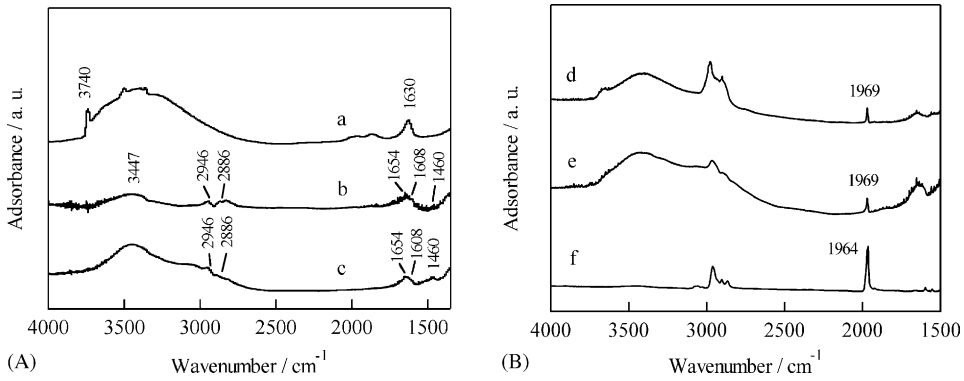

Fig. 1. FT-IR spectra for (a) MCM-41; (b) 1N-MCM-41; (c) 2N-MCM-41; (d) Rh–P**2**/1N-MCM-41; (e) Rh–P**2**/2N-MCM-41; and (f) RhCl(CO)(P**2**)$_2$.

Philips TECNAI F-30 FEG instrument using accelerating voltage of 300 kV. The sample was dispersed in dry ethanol with an ultra-sonic machine and then deposited on a copper grid with a holey carbon film. Chemical compositions were examined by EDS using a TECNAI F-30 FEG electron microscope operated at 300 kV. Table 1 lists the structural property and elemental analysis data for MCM-41 and MCM-48 before and after amino-functionalization.

2.4. Hydroformylation

The typical olefin hydroformylation was carried out in a stainless steel autoclave of 60 ml with a magnetic stirrer. After the introduction of required amount of the catalyst, olefin and toluene were placed in the autoclave. The reactor was then pressurized three times with 1.0 MPa of CO/H_2 (1/1, v/v). Then the autoclave was pressurized with the same gas mixture at a desirable pressure, and heated to the reaction temperature. After the reaction, the reactor was cooled with an ice bath and decompressed. The oils and the catalysts were separated by centrifugation. The organic phase was analyzed with a gas chromatograph equipped with FID and a capillary column (SE-30, 30 m × 0.32 mm × 0.25 μm).

Table 2
Carbonyl vibrations for the Rh–P complexes before and after immobilization

Ligand	Cone angle (θ)	ν_{CO} (cm^{-1})		
		Rh–P	Rh–P/1N-MCM-41	Rh–P/2N-MCM-41
PPh_3	146	1964	1967	1969
1	152	1964	1967	1969
2	159	1964	1969	1969

3. Results and discussion

3.1. Characterization of FT-IR, XRD, BET and HRTEM

Fig. 1(a) shows the IR spectra for MCM-41 before and after amino-functionalization. A very broad absorption band centered at 3431 cm^{-1} assigned to hydrogen-bonded Si-OH groups was perturbed by physically adsorbed water, while a sharp absorption is observed at 3740 cm^{-1} ascribed to free Si-OH groups [26–29]. After amino-functionalization with $NH_2(CH_2)_3Si(OEt)_3$ or $NH_2CH_2CH_2NH(CH_2)_3Si(OMe)_3$, the band at 3740 cm^{-1} for free Si-OH groups was depleted greatly at the expense of the appearances of bands at 2946, 2886, 1654, 1608, 1460 and 1408 cm^{-1}, which are assigned to C–H asymmetric stretching, C–H symmetric stretching, NH_2 scissor, NH_2 scissor, CH_2 scissor, and CH_3 bending vibrations, respectively. The band positions are similar to those reported in the literature [29–31]. The above IR spectroscopic results suggested that the significant condensation occurred between the OH groups at the surface of MCM-41 and the aminoalkyltrialkoxysilanes.

The cone angles of *tert*-butyl-substituted phosphines **1** and **2** are larger than that of PPh_3, but electronically these three ligands show no great difference (Table 2).

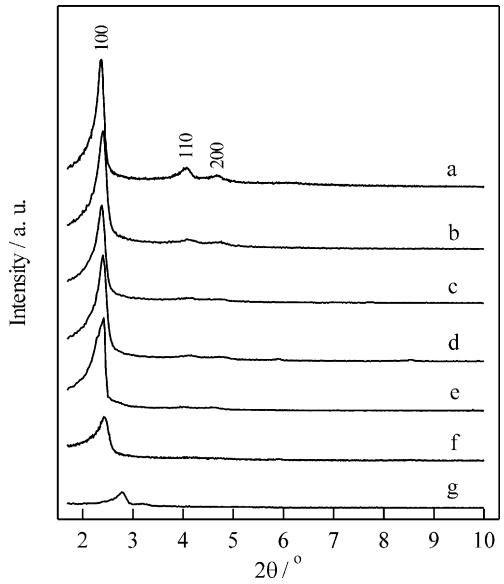

Fig. 2. XRD patterns for supports and catalysts (a) MCM-41; (b) 1N-MCM-41; (c) Rh–P**1**/1N-MCM-41; (d) Rh–P**2**/1N-MCM-41; (e) 2N-MCM-41; (f) Rh–P**1**/2N-MCM-41; and (g) Rh–P**2**/2N-MCM-41.

The catalysis in homogeneous system has revealed that the non-coordinating *tert*-butyl group in phosphines was able to act as steering "arms" for the substrate and thus affected the conversion and product distribution [22]. Fig. 1(b) shows the IR spectra for Rh–P**2**, Rh–P**2**/1N-MCM-41 and Rh–P**2**/2N-MCM-41, respectively. The band at 1964 cm^{-1} represented the carbonyl vibration of crystalline Rh–P**2**. The samples of Rh–P**2**/1N-MCM-41 and Rh–P**2**/2N-MCM-41 gave a similar carbonyl vibration at 1969 cm^{-1}. The small shift in the carbonyl wavenumber might be ascribed to the slight deformation or the ligand exchange in the Rh-complex in the process of heterogenization. Analogous observations were obtained for the samples of Rh–P**1**/1N-MCM-41 and Rh–P**1**/2N-MCM-41 as listed in Table 2.

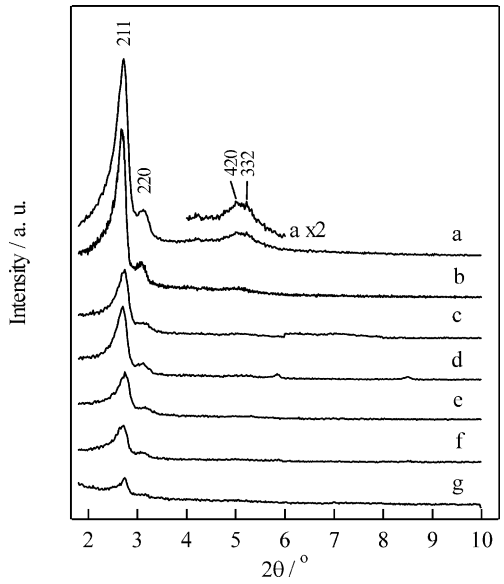

Fig. 3. XRD patterns for supports and catalysts (a) MCM-48; (b) 1N-MCM-48; (c) Rh–P**1**/1N-MCM-48; (d) Rh–P**2**/1N-MCM-48; (e) 2N-MCM-48; (f) Rh–P**1**/2N-MCM-48; and (g) Rh–P**2**/2N-MCM-48.

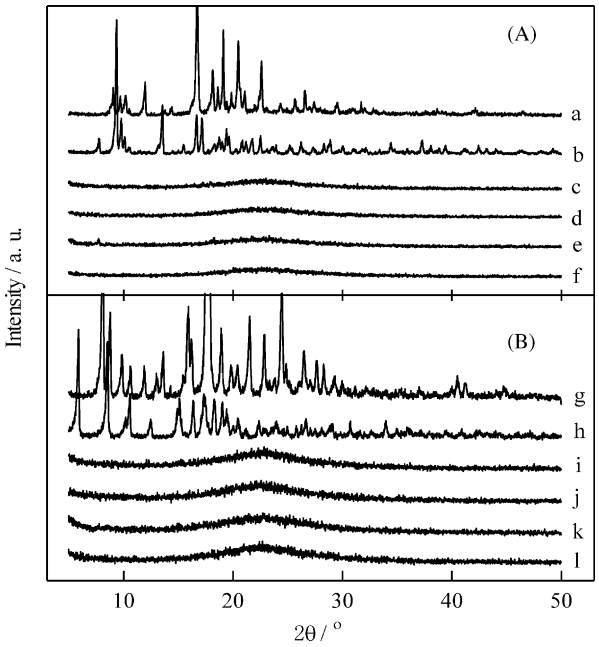

Fig. 4. Large angle XRD patterns of various catalysts (a) P**1**; (b) $RhCl(CO)(P\mathbf{1})_2$; (c) Rh–P**1**/1N-MCM-41; (d) Rh–P**1**/2N-MCM-41; (e) Rh–P**1**/1N-MCM-48; (f) Rh–P**1**/2N-MCM-48; (g) P**2**; (h) $RhCl(CO)(P\mathbf{2})_2$; (i) Rh–P**2**/1N-MCM-41; (j) Rh–P**2**/2N-MCM-41; (k) Rh–P**2**/1N-MCM-48; and (l) Rh–P**2**/2N-MCM-48.

Figs. 2 and 3 compare the X-ray diffraction patterns for MCM-41 and MCM-48 before and after the aminoalkylsilane-functionalization and the immobilization of Rh–P complexes, respectively. Aminoalkylsilane grafted to MCM-41 or MCM-48 and further immobilizing Rh–P

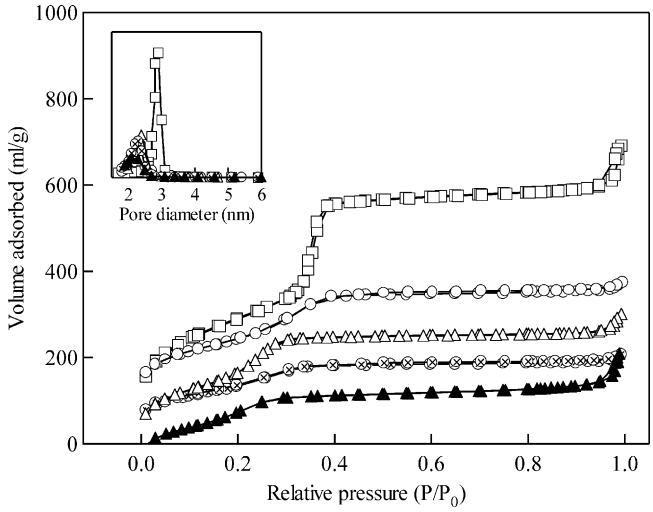

Fig. 5. N_2 adsorption isotherms and BJH pore-size distribution. (□): MCM-41; (○): 1N-MCM-41; (△): 2N-MCM41; (⊗): Rh–P**1**/1N-MCM41; (▲): Rh–P**2**/2N-MCM41.

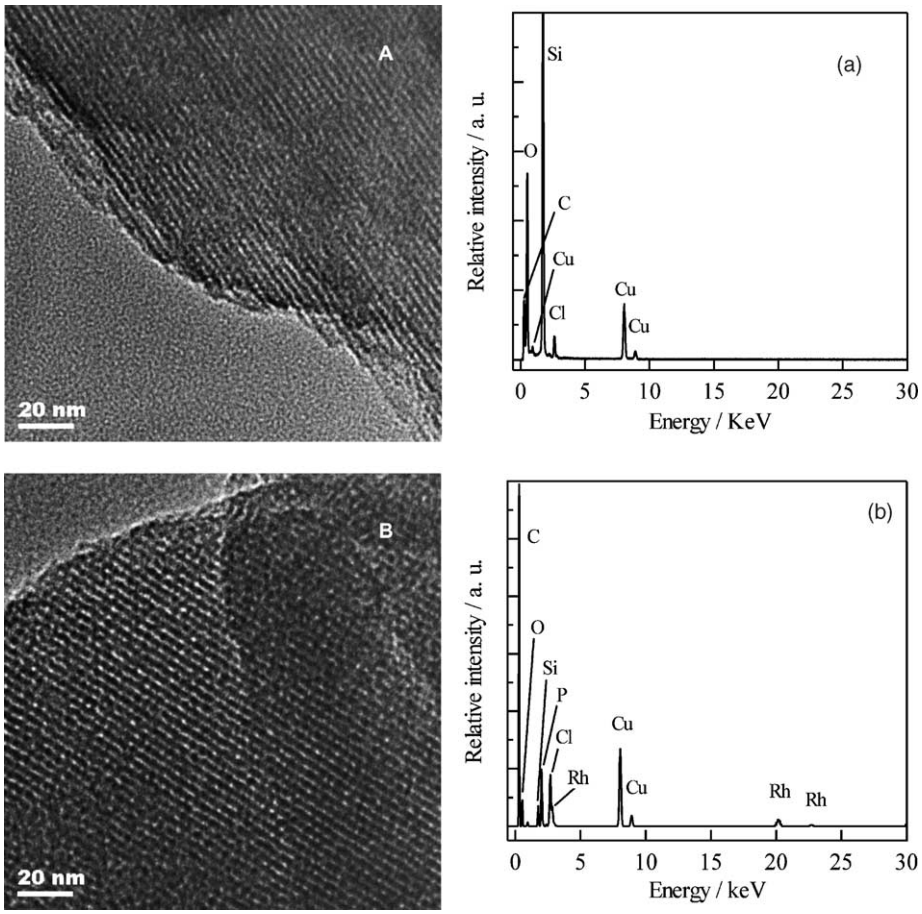

Fig. 6. The HRTEM images with corresponding EDS patterns for (a) 2N-MCM-41; (b) Rh–P**2**/2N-MCM-41.

on aminoalkylsilane-grafted ones caused a considerable decrease in the XRD intensity and the peak positions slightly shifted to higher 2θ (degree). The peaks at higher indices almost disappeared and also the (1 0 0) peak became weak for the samples after the immobilization of Rh–P complexes. These changes might be due to a partial loss of the space correlation of the pores and were commonly observed in studies of silylation of mesoporous silicas [26]. On the other hand, few differences in the XRD patterns were observed for the catalysts before and after six runs of 1-hexene hydroformylation, indicating that the 2D-hexagonal/cubic structures of the catalysts were stable under the catalytic reaction.

The large angle powder XRD patterns for a series of heterogenized catalysts are illustrated in Fig. 4. The XRD patterns for the heterogenized ones showed almost no lines for the ligands and the crystalline complexes of Rh–P**1** and Rh–P**2**, suggesting that the Rh-complexes interact conceivably with the amino groups at the surfaces of mesoporous silicas and be highly dispersed at the surfaces.

The N_2 adsorption–desorption isotherms for the as-prepared samples of MCM-41, 1N-MCM-41, 2N-MCM-41, Rh–P**1**/1N-MCM-41 and Rh–P**2**/2N-MCM-41 are shown in Fig. 5. The BET surface area (S_{BET}) and BJH pore diameter are given in Table 2. The pure-silica MCM-41 displayed a type IV isotherm with H1 hysteresis and a sharp increase in volume adsorbed at $P/P_0 = 0.4$, characteristic of highly ordered mesoporous materials. For the amino-functionalized samples and the corresponding catalysts, they exhibited a type IV isotherm with a lower specific surface area and a slightly smaller pore volume. The BJH pore size calculated from the adsorption branches was also smaller than that of MCM-41. These results revealed that the considerable amounts of amino groups and the complexes of Rh–P**1** and Rh–P**2** were mostly located in the inner channel of mesoporous supports.

Fig. 6 shows the HRTEM images and their EDS patterns for the as-prepared samples of 2N-MCM-41 and Rh–P**2**/2N-MCM-41. It was found that no dramatic differences could be observed among the images of MCM-41 (not shown), 2N-MCM-41 and Rh–P/2N-MCM-41, but the EDS for Rh–P**2**/2N-MCM showed the existence of Rh atom and phosphorous species, giving the molar ratio of P/Rh of about 1.88. We screened three points of the sample for the EDS patterns and found no significant differences. These indicted that the whole characteristic features of the regular hexagonal array were essentially retained in the functionalized MCM-41 and the catalyst thus prepared,

Table 3
Activity and selectivity of hydroformylation of 1-hexene with various catalysts

Catalyst	S_{BET} ($m^2\ g^{-1}$)	Pore size (nm)	Rh content (wt.%)	Time (h)	Conversion (%)	*n/i*	TOF (h^{-1})
$RhCl(CO)(P\mathbf{1})_2$	–	–	–	0.5	44.2	1.3	568
$RhCl(CO)(P\mathbf{2})_2$	–	–	–	0.5	49.3	1.8	720
$RhCl(CO)(PPh_3)_2$	–	–	–	0.5	43.1	1.2	525
Rh–P**1**/MCM-41	990	2.6	0.43	1	14.2	1.7	270
Rh–P**2**/MCM-41	951	2.7	0.38	1	12.0	2.0	255
Rh–P**1**/1N-MCM-41	634	2.4	1.38	1	67.5	1.4	402
Rh–P**2**/1N-MCM-41	662	2.4	0.77	1	83.4	1.8	891
Rh–P**1**/2N-MCM-41	538	2.3	1.10	1	75.5	1.8	562
Rh–P**2**/2N-MCM-41	539	2.4	0.72	1	62.3	2.4	712
$Rh–PPh_3$/2N-MCM-41	475	2.5	1.82	1	74.2	1.3	334
Rh–P**1**/MCM-48	655	2.3	0.38	1	14.5	0.8	314
Rh–P**2**/MCM-48	658	2.5	1.90	1	35.2	1.0	150
Rh–P**1**/1N-MCM-48	501	2.6	2.02	1	84.0	1.3	342
Rh–P**2**/1N-MCM-48	546	2.3	0.62	1	74.5	1.6	981
Rh–P**1**/2N-MCM-48	334	2.4	0.96	1	82.6	1.8	707
Rh–P**2**/2N-MCM-48	286	2.3	1.06	1	80.0	2.5	620
$Rh–PPh_3$/2N-MCM-48	238	2.6	1.31	1	51.2	1.4	321

Reaction conditions: $RhCl(CO)(L)_2$ = 10 mg (0.0125 mmol for $RhCl(CO)(P\mathbf{1})_2$, 0.0109 mmol for $RhCl(CO)(P\mathbf{2})_2$, and 0.0145 mmol $RhCl(CO)(PPh_3)_2$), immobilized sample: 100 mg, total pressure: 2.0 MPa (H_2/CO = 1/1, v/v), agitation speed: 800 rpm, reaction temperature: 373 K, 1-hexene: 1 ml (8 mmol), toluene: 15 ml (140.8 mmol).

and that the dispersion of the Rh–P complexes at the surfaces of amino-functional mesoporous silicas was uniform and homogeneous under the present preparation conditions. The molar ratio of P**2**/Rh in the Rh–P**2**/2N-MCM-41 from the EDS was close to the stoichiometric value in the precursor of $RhCl(CO)(P\mathbf{2})_2$, suggesting that the sample of Rh–P**2**/2N-MCM-41 might be electronically similar to $RhCl(CO)(P\mathbf{2})_2$ as illustrated in Scheme 1. The result was in conformity with the FTIR observation where the carbonyl wavenumber for Rh–P**2**/2N-MCM-41 was only shifted to a slightly higher wavenumber as compared to that for $RhCl(CO)(P\mathbf{2})_2$.

3.2. Hydroformylation of 1-hexene

In homogeneous systems, the complex with phosphines **1** and **2** bearing the bulk *tert*-butyl group(s) in the *para*-position of phosphorus atom have shown advantages over PPh_3 in the product selectivity towards the normal heptanal in the hydroformylation of 1-hexene due to the larger cone angle of the ligands. A comparison of 1-hexene hydroformylation over a series of catalysts has been listed in Table 3. The results of homogeneous catalysis are also incorporated in the table. In all cases, the aldehyde selectivity in 1-hexene hydroformylation was higher than 96% and the hydrogenation product of 1-hexene was less than 4%. Moreover, no heptanols were detected by the capillary GC. When Rh–P**1** or Rh–P**2** was directly immobilized on the non-functionalized MCM-41 or MCM-48, the lower catalytic performance was obtained as reflected by the 1-hexene conversion and the heptanal *n/i* ratio. In contrast to this, when Rh–P**1** or Rh–P**2** was immobilized on the amino-functionalized MCM-41 or MCM-48, the catalysts afforded higher conversion and also improved selectivity to normal heptanal, particularly in the cases using 2N-MCM-41 and 2N-MCM-48 as supports. These results were probably due to the interaction between the Rh–P complexes and the surface amino-groups and the resulting high dispersion of the active Rh-species at the catalyst surfaces as evidenced by XRD and HRTEM. It was also found that the Rh–P**2** immobilized on amino-functionalized MCM-41 and MCM-48 provided an improved selectivity to normal heptanal than Rh–P**1** immobilized on the same ones. As a results, the highest selectivity to heptanal was obtained with Rh–P**2**/2N-MCM-41 and Rh–P**2**/2N-MCM-48 catalysts.

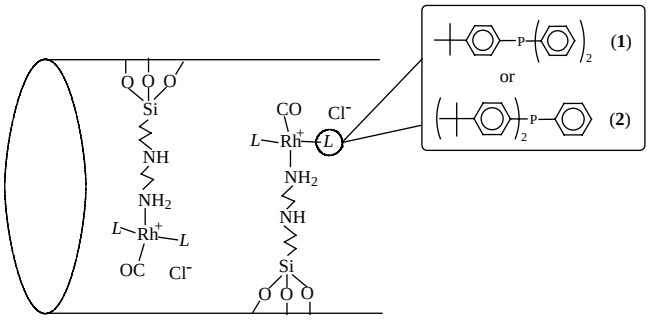

Scheme 1. Possible structure for Rh–P**1**/2N-MCM-41 or Rh–P**2**/2N-MCM-41.

The recycling of the catalysts prepared by immobilization of Rh–P**2** on MCM-41, 2N-MCM-41 and 2N-MCM-48 was performed through a series of consecutive runs for 1-hexene hydroformylation. The results are presented in Fig. 7. The catalyst Rh–P**2**/MCM-41, which was prepared by the direct immobilization of Rh–P**2** on the non-functionalized MCM-41, deactivated quickly due to the severe leaching of Rh species during the reactions, as observed by the yellowish color of the organic product. The Rh–P**2**/2N-MCM-41

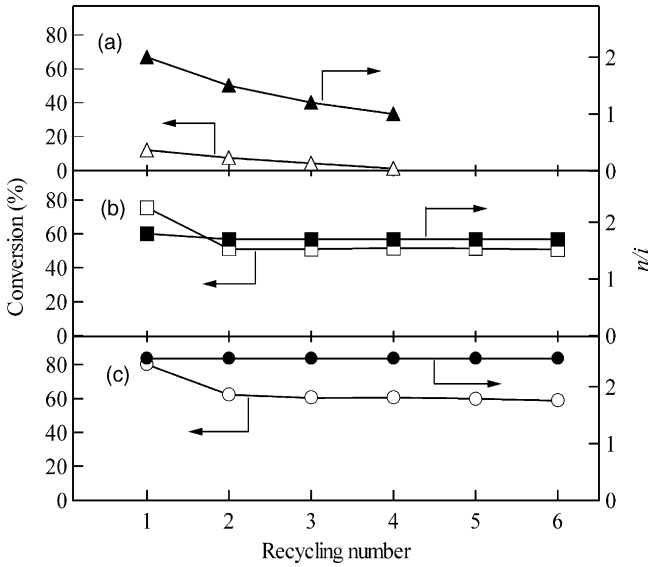

Fig. 7. The recycling results in 1-hexene hydroformylation over catalysts (a) Rh–P**2**/MCM-41; (b) Rh–P**2**/2N-MCM-41; and (c) Rh–P**2**/2N-MCM-48. Reaction conditions: Rh content for (a) 0.38 wt.%, (b) 0.72 wt.% and (c) 1.06 wt.%; reaction time 2 h. Other conditions are the same as in Table 2.

and the Rh–P**2**/2N-MCM-48, however, exhibited rather good catalytic stability. With the exception of the remarkable decrease in the first recycle, the catalytic performance remained almost unchanged in the next several runs. This is likely due to the reason that some amounts of Rh–P species were anchored at the outer surface of the functional mesoporous silicas and thus readily leached off and dissolved into the organic phase during the first run of hydroformylation. The above results indicated that there existed extensive interactions between the supports and the Rh–P complexes.

4. Conclusion

The whole characteristic features of the regular hexagonal or cubic arrays were retained in the organo-functionalized mesoporous silicas MCM-41 or MCM-48, and the encapsulated catalysts were thus prepared before and after catalytic hydroformylation. The Rh–P complexes were uniformly and highly dispersed at the surfaces of amino-functionalized mesoporous silicas. These heterogenized catalysts showed comparable catalytic activity and normal heptanal selectivity in comparison with the corresponding homogeneous ones. Better hydroformylation performance was obtained by attaching Rh–P**2** complex to the amino-funcationalized mesoporous silicas. The improvement in activity might be due to the high dispersion of Rh–P complexes through a chemical interaction with the surface amino-groups at MCM-41 and MCM-48, while the enhancement in the product selectivity towards the normal heptanal might be principally ascribable to the contribution of larger cone angle of the ligands **1** and **2** over Rh–PPh_3 and also to the confinement of pore sizes after amino-grafting at the mesoporous silicas as well.

Acknowledgements

The authors greatefully acknowledge the financial supports from the National Basic Research Priorities Programme (973-project) (G2000048008), the NSF of China (20023001 and 20021002).

References

[1] B. Cornils, W.A. Herrmann, Applied Homogeneous Catalysis with Organometallic Compounds, VCH, New York, 1996.
[2] F.R. Hartley, Supported Metal Complexes, D. Reiel Publishing Company, Dordrecht, 1985.
[3] H. Gao, R.J. Angelici, J. Am. Chem. Soc. 119 (1997) 6937.
[4] H. Yang, H. Gao, R.J. Angelici, Organometallics 19 (2000) 622.
[5] C. Bianchini, V. Dal Santo, A. Meli, S. Moneti, M. Morento, W. Oberhauser, et al., Angew. Chem. Int. Ed. 42 (2003) 2636.
[6] H. Gao, R.J. Angelici, J. Mol. Catal. A: Chem. 145 (1999) 83.
[7] J.S. Beck, J.C. Vartuli, W.J. Roth, M.E. Leonowicz, C.T. Kresge, K.D. Schmitt, et al., J. Am. Chem. Soc. 114 (1992) 10834.
[8] D.E. De Vos, M. Dams, B.F. Sels, P.A. Jacobs, Chem. Rev. 102 (2002) 3615.
[9] X.G. Zhou, X.Q. Yu, J.S. Huang, S.G. Li, L.S. Li, C.M. Che, Chem. Commun. (1999) 1789.
[10] H.H. Wagner, H. Hausmann, W.F. Hölderich, J. Catal. 203 (2001) 150.
[11] S. Xiang, Y.L. Zhang, Q. Xin, C. Li, Chem. Commun. (2002) 2696.
[12] C. Merckle, S. Haubrich, J. Blümel, J. Organomet. Chem. 627 (2001) 44.
[13] C.M. Crudden, D. Allen, M.D. Mikoluk, J. Sun, Chem. Commun. (2001) 1154.
[14] H.M. Hultman, M. De Lang, I.W.C.E. Arends, U. Hanefeld, R.A. Sheldon, T. Maschmeyer, J. Catal. 217 (2003) 275.
[15] C. Merckle, J. Blümel, Adv. Synth. Catal. 345 (2003) 584.
[16] M.D. Jones, R. Raja, J.M. Thomas, B.F.G. Johnson, D.W. Lewis, J. Rouzaud, et al., Agnew. Chem. Int. Ed. 42 (2003) 4326.
[17] Y. Cai, Z.H. Li, Y.Q. Yang, Y.Z. Yuan, Chem. Res. Chinese Univ. 18 (2002) 311.
[18] K. Mukhopadhyay, A.B. Mandale, R.V. Chaudhari, Chem. Mater. 15 (2003) 1766.
[19] Y. Yang, Q.R. Peng, Y.Z. Yuan, Chinese J. Catal. 25 (5) (2004) in press.
[20] L. Huang, J.C. Wu, S. Kawi, J. Mol. Catal. A: Chem. 206 (2003) 371.
[21] L. Caron, M. Canipelle, S. Tilloy, H. Bricout, E. Monflier, Tetrahedron Lett. 42 (2001) 8837.
[22] Q.R. Peng, Y. Yang, Y.Z. Yuan, Catal. Lett. 88 (3–4) (2003) 219.
[23] L.Y. Chen, T. Horiuchi, T. Mori, K. Maeda, J. Phys. Chem. B 103 (1999) 1216.
[24] K. Mukhopadhyay, B.R. Sarkar, R.V. Chaudhari, J. Am. Chem. Soc. 124 (2002) 9692.
[25] H. Yoshitake, T. Yokoi, T. Tatasumi, Chem. Mater. 15 (2003) 1713.
[26] J.S. Chen, Q.H. Li, R.R. Xu, F.S. Xiao, Angew. Chem. Int. Ed. 34 (1995) 2694.
[27] X.S. Zhao, G.Q. Lu, A.J. Whittaker, G.J. Millar, H.Y. Zhu, J. Phys. Chem. B 101 (1997) 6525, and references therein.
[28] A. Jentys, N.H. Pham, H. Vinek, J. Chem. Soc. Faraday Trans. 92 (1996) 3287.
[29] J.F. Diaz, K.J. Balkus, Chem. Mater. 9 (1997) 61.
[30] D.H. Park, S.S. Park, S.J. Choe, Bull. Korean Chem. Soc. 20 (1999) 291.
[31] H. Yoshitake, T. Yokoi, T. Tatsumi, Chem. Mater. 14 (2002) 4603.